Graph neural networks predict energetic and mechanical properties for models of solid solution metal alloy phases

Massimiliano Lupo Pasini*,[a], Gang Seob Jung[a], Stephan Irle[a]

[a] *Oak Ridge National Laboratory, Computational Sciences and Engineering Division, 1 Bethel Valley Road, Oak Ridge, TN, USA, 37831*

Abstract

We developed a PyTorch-based architecture called HydraGNN that implements graph convolutional neural networks (GCNNs) to predict the formation energy and the bulk modulus for models of solid solution alloys for various atomic crystal structures and relaxed volumes. We trained the GCNN surrogate model on a dataset for nickel-niobium (NiNb) generated by the embedded atom model (EAM) empirical interatomic potential for demonstration purposes. The dataset was generated by calculating the formation energy and the bulk modulus as a prototypical elastic property for optimized geometries starting from initial body-centered cubic (BCC), face-centered cubic (FCC), and hexagonal compact packed (HCP) crystal structures, with configurations spanning the possible compositional range for each of the three types of initial crystal structures. Numerical results show that the GCNN model effectively predicts both the formation energy and the bulk modulus as function of the optimized crystal structure, relaxed volume, and configurational entropy of the model structures for solid solution alloys.

Key words: Solid Solution Alloys, Condensed Matter, Bulk Modulus, Deep Learning, Graph Neural Networks

.

This manuscript has been authored in part by UT-Battelle, LLC, under contract DE-AC05-00OR22725 with the US Department of Energy (DOE). The US government retains and the publisher, by accepting the article for publication, acknowledges that the US government retains a nonexclusive, paid-up, irrevocable, worldwide license to publish or reproduce the published form of this manuscript, or allow others to do so, for US government purposes. DOE will provide public access to these results of federally sponsored research in accordance with the DOE Public Access Plan (`http://energy.gov/downloads/doe-public-access-plan`).

1. Introduction

The development of new alloy materials with desired properties is a time-consuming process that requires exhaustive experimental investigations into elemental compositions and processing conditions. These investigations are traditionally carried out in a trial-and-error manner [1, 2]. The properties of alloys are mainly governed by their composition, phase, and by the manner individual crystalline regions known as "grains" are arranged in the microstructure. Therefore, structural variability in alloys spans multiple scales, from the atomic to the macroscale, giving rise to a myriad of possible alloy systems. Just the elemental composition alone represents a combinatorically complex problem since finding the optimal mixture requires exploring a high dimensional materials space defined by a wide range of chemical compositions and atomic configurations for each of them. Finding new compositions and microstructures for alloys with desired properties is therefore not amenable to traditional random search approaches [1, 2]. This simple fact has led to a situation where modern technologies only utilize a tiny fraction of potentially interesting alloys.

Computational modeling and artificial intelligence (AI) have emerged as valuable tools to accelerate this process by simulation and prediction for a wide variety of design factors [3]. Thermal effects on the stability of the different phases, their phase transformations, and equilibrium geometries, among others,

*Corresponding author
Email address: `lupopasinim@ornl.gov` (Massimiliano Lupo Pasini)

are prominent factors hampering the computational design of alloy systems and processes. Nevertheless, progress has been made in recent years, and alloy properties that are nowadays frequently optimized include yield stress, ultimate tensile strength, and oxidation resistance [4]. Due to the complexity of actual alloy processing, the CALPHAD (CALculation of PHAse Diagrams) method [5, 6], combining experimental data and theoretical results based on thermodynamic Gibbs energy, has been widely utilized to design complicated alloy systems such as solid-solution high entropy alloys. Its Gibbs free energy functions describing an alloy system are indirectly obtained from experiments, with the caveat that probing all possible combinations of alloy elements through experimental measurement is prohibitive. An additional restriction in CALPHAD is that alloy nanoparticle design with a resolution greater than 5 nm is generally not allowed [7]. Recently, mesoscale AI models have been developed to partially alleviate these limitations [8].

On the microscale, atomistic thermodynamic modeling can provide energy information and often is utilized to gain information missing in CALPHAD [7, 9]. The influence of atomic disorder on thermodynamic and mechanical properties has already been explored computationally [10, 11, 12, 13] for various families of crystalline materials including solid solution alloys. Given N lattice sites and p possible pure element types at each site, the dimensionality of the material space characterizing solid solution alloys scales like p^N, which explodes for increasing values of N and/or p. A thorough and time-efficient exploration of such a high-dimensional space requires fast (but still accurate) evaluations of the target property for every possible atomic arrangement. While state-of-the-art *ab initio* simulations, e.g. based on density functional theory (DFT), can yield highly accurate energetics and mechanical properties, their computational requirements still prohibit a thorough sampling of vast ranges of chemical composition and atomic configurations, even considering the computational power of massively parallel leadership supercomputers. Also, atomistic modeling of metal alloys is challenging because for non-stoichiometric compositions they are likely to form a disordered solid solution, and one needs to properly account for configurational entropy. Large-scale computational databases such as the Materials Project [14], the Open Quantum Materials Database (OQMD) [15], and the AFLOW-lib [16] database do not cover structures for sufficiently broad ranges of stoichiometry to cover relevant atomic configurations occuring in solid solution alloys.

Lattice-based models (e.g., cluster expansion [17]) where the atomic positions are fixed are able to accurately account for the configurational entropy. These models can be combined with Monte Carlo (MC) simulations to perform thermodynamic averages to search for optimal structures. However, the contribution of configurational entropy in the total entropy at the high temperature is sometimes small ($\approx$15% in a previous study [18]), and vibrational contributions are not generally handled in lattice models [19]. Off-lattice models, e.g., interatomic potentials, utilize the details of atomic coordinates for the quantities. MC and molecular dynamics (MD) techniques with the interatomic potentials, e.g., modified embedded atom method (MEAM), are utilized to sample reliable atomic configurations and identify phase stability [20, 21].

Data-driven modeling techniques allow for inexpensive and accurate predictions of material properties and thereby enable rapid screenings of large material search spaces to select potential material candidates with desirable properties [22, 23, 24, 25, 26, 27, 28, 1]. In particular, deep learning (DL) models have the potential to accurately represent complex relations between input features and target quantities, but require large volumes of training data to attain high accuracy. Graph convolutional neural networks (GCNNs) are a particular type of DL models, well suited to process data represented as graph samples. Currently, GCNN models are used as surrogates in material science to predict material properties from atomic information by directly mapping the atomic structure input to graphs, with atoms as graph nodes and chemical bonds, or nearest-neighbor interactions, as edges [29, 30].

Previous work with GCNN surrogate models in materials science includes crystal graph convolutional neural networks (CGCNN) [29] and material graph network (MEGNet) [30]. The focus of these efforts was on using GCNNs for prediction of material properties across broad classes of stoichiometric, intermetallic, and ordered crystalline materials, sourced from the Materials Project and the Open Quantum Materials Database (OQMD) [31, 32]. This work showed significant flexibility of GCNNs, simultaneously handling many materials across different properties, with good accuracy relative to the original density functional theory (DFT) results. More recent work started investigating the effectiveness of GCNN models for prediction of mixing enthalpy, atomic charge transfer, and atomic magnetic moment for solid solution ferromagnetic alloys, characterized by disordered atomic configurations, with non-relaxed crystal structure and fixed volume from open-source DFT data [33, 34]. Results showed that the GCNN model can accurately estimate material properties as a function of the configurational entropy [35, 36].

In this work, we extend the use of GCNNs to predicting the formation energy and bulk modulus as a prototypical elastic property of solid solution alloys for disordered atomic configurations in different types of optimized crystal structures with fully relaxed volumes that span the possible compositional range of the binary alloy. As an illustration, we train the GCNN model on an open-source dataset for the nickel-niobium (Ni-Nb) alloy that provides formation energy and bulk modulus calculated with the embedded atom model (EAM) empirical potential [37] for several atomic configurations with optimized crystal structures. We investigate the performance of the GCNN with respect to the radius cutoff, which determines the size and thereby the computer time and memory requirements of the surrogate model, as well as two different graph convolutional layers that are implemented in the Pytorch-Geometric open-source library, namely CGConv and PNAConv, and report the mean absolute errors (MAEs) for combinations of cut-off radius and GCNN type. Our numerical results show that the GCNN model is able to learn the dependency of formation energy and the bulk modulus with respect to the crystal structure over the possible compositional range, but the prediction of bulk modulus is affected by greater deviations from ground truth data than energy predictions.

2. Computational methodology

2.1. Graph convolutional neural networks

GCNNs [38, 39] are DL models for processing graph data. Representing crystal structures in the form of graphs is natural since the atoms can be viewed as nodes and metallic bonds as edges of the graph. Nodes in the graph retain atomic features in crystal structures and edges in the graph retain the connectivity and (optionally) the mutual distance between nodes. Each graph associated with a specific crystallographic structure can have global graph-level properties such as the formation energy and the bulk modulus.

Graph convolutional layers

Graph convolutional layers are the core of GCNNs and are used to collect information from neighboring nodes using a message-passing framework. The characterization of the neighborhood is performed through a radius cutoff, which is a hyperparameter of the GCNN model. Each node representing an atom in the structure is connected through an edge to all neighboring nodes within a distance shorter than the radius cutoff, whereas interactions with atoms with a distance longer than the radius-cutoff are disregarded. Even though metallic bonds are characterized by a "sea" of delocalized valence electrons, the cohesive bonding strength nevertheless is strongly determined by the immediate interactions with nearby atoms. Thus forcing nodes in the graph to be locally connected to all neighbouring atoms within a sphere determined by the radius cutoff accurately mimics the physics of metallic alloys.

Through consecutive steps of message passing, the graph nodes gather information from nodes that are further and further away, which implicitly accounts for many-body interactions. Global pooling layers are connected at the end of a stack of consecutive graph convolutional layers and aim at aggregating the node feature associated with each atom across a graph into a single feature. This is achieved by summing the local interactions of each atom with its neighbors and using the result to estimate global properties. Finally, fully connected (FC) layers take the results of pooling, i.e., the extracted features, and provide the output prediction for global properties.

Differing in the policy adopted to aggregate, transfer, and update nodal information through the message passing policy, a variety of GCNNs have been developed, namely crystal GCNNs (CGCNN) [29], and principal neighborhood aggregation (PNA) [40]. Their corresponding graph convolutional layers are provided by the open-source PyTorch Geometric library [41], namely CGConv and PNAConv, and can be used by our implementation of GCNN models called HydraGNN [42]. CGConv and PNAConv differ in the policy used to update node features using information coming from adjacent nodes in the graph. CGConv was specifically developed for atomic crystals, and uses the sum operator to aggregate information from adjacent nodes, whose importance is tuned via a learnable scaling factor. PNAConv combines multiple aggregation policies (e.g., mean, maximum, minimum, standard deviation) to enhance the discriminative power of the model in distinguishing different messages when using a graph convolutional layer, thus resulting in a better preservation of graph isomorphism. Similarly to CGConv, PNAConv also relies on learnable scaling operators to assign different importance to different adjacent nodes.

3. Solid solution binary alloy dataset

In this work we focus on models for a solid solution binary alloy, where two constituent elements are randomly placed on an underlying crystal lattice with pre-defined unit cell size. Nickel-niobium is one example where niobium and other metal elements are mixed in varying compositions to produce special nickel (Ni) steels and nickel-based super alloys. Niobium (Nb) enhances the mechanical properties, creep resistance and weldability of steels and super alloys [43]. We therefore created and used a dataset for Ni-Nb alloys based on the EAM potential [44] and made it available through the OLCF Constellation [45]. The potential developed in [44] could describe behaviors of the liquid and solid phases of $Ni_{62}Nb_{38}$ alloy. The developed EAM potential was extensively tested with ab-initio MD simulations regarding to the pair distribution functions at a high temperature such as T=1447K. Also, the bond length and angle distributions are with those from ab-initio calculations, showing good agreements. They also measure in-situ X-ray scattering of the liquid phase of $Ni_{62}Nb_{38}$ alloy. Due to the extensive tests on the amorphous and liquid phase during the development, we utilized the EAM potential for randomly selected solid-solution atomic structures. The dataset includes both the formation energy as well as the bulk modulus for each alloy composition and structure. Each atomic sample has a disordered phase which is obtained starting from an initial regular crystal structure of type body-centered cubic (BCC), face-centered cubic (FCC), or hexagonal compact packed (HCP). Geometry optimization were performed using the LAMMPS simulation package [46] to ensure that all the alloy samples reached an equilibrium geometry, characterized by negative formation energies relative to isolated atoms. The EAM potential is a reasonable choice for our purposes as it describes well the behaviors of the liquid and solid phases of Ni-Nb alloy [44]. The structural factors and angular distributions of three atoms are well-matched with X-ray and *ab initio*-based molecular dynamics data. We prepared the three different crystals with different initial lattice parameters (3.52 Å for FCC, 3.32 Å for BCC, and 3.5 Å for HCP). We performed energy minimization in two steps. Firstly, we minimized the structures with an isotropic unit cell to minimize the side effects from our arbitrary lattice parameters for all other compositions. Then, we applied geometry optimization with a triclinic (non-orthogonal) unit cell to fully minimize the stress components to calculate the elastic constants. In this procedure, we chose 10,000 as the maximum number of allowable steps aimed at obtaining fully relaxed atomic geometries. Figure 1 shows examples of relaxed geometries of initially BCC (a), FCC (b), and HCP (c) with different compositions.

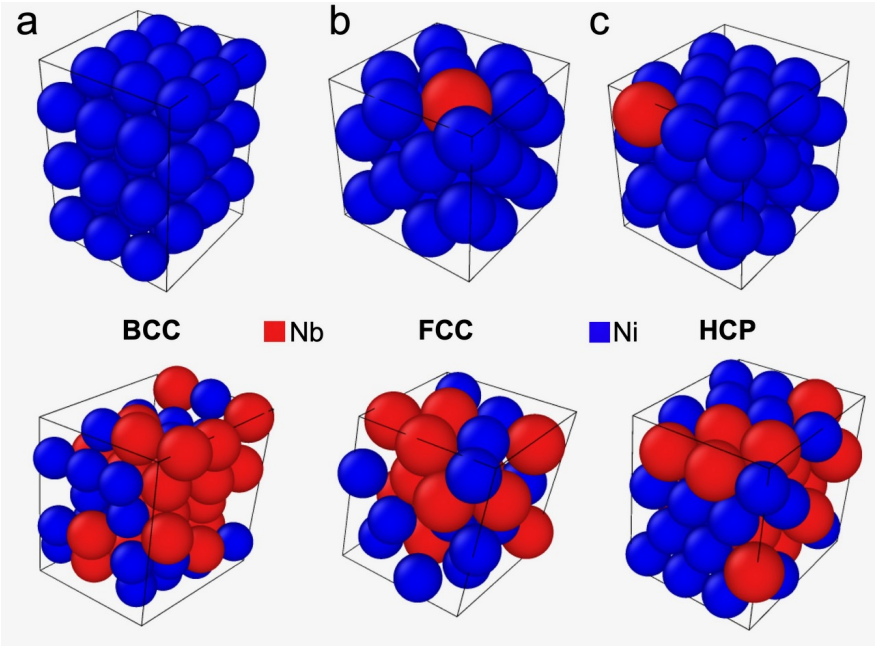

Figure 1: Snapshots of relaxed geometries of initially BCC (a), FCC (b), and HCP (c) with different compositions. Top panels have only one Nb in Ni matrix showing well-ordered structures in orthogonal simulation boxes. Bottom panels have similar ratios between Ni and Nb compositions, showing non-orthogonal simulation boxes, which are difficult to be defined as a specific crystal structure.

The input to the GCNN model for each sample includes the three components of the atom position and the atomic number. The predicted values are the formation energy and the bulk modulus. The dataset consists of three sets of crystal structures. The first set contains $46,086$ irregular crystal structures, each of them with 54 atoms, obtained through topology optimization starting from a regular BCC crystal structure. The second set contains $24,543$ irregular crystal structures, each of them with 32 atoms, obtained through topology optimization starting from a regular FCC crystal structure. The third set contains $39,303$ irregular crystal structures, each of them with 48 atoms, obtained through topology optimization starting from a regular HCP crystal structure. The atomic configurations within each set span the possible compositional range. The three sets have been merged into a global dataset, which is extremely heterogeneous in terms of crystal structures, lattice volumes, and atomic configurations. In order to ensure each composition is adequately represented in all portions of the dataset, splitting between the training, validation, and test sets was done separately for each composition.

In the ground state, the total energy E of an alloy can be written as

$$E = \sum_{i=1}^{N_{\text{elem}}} c_i E_i + \Delta E_{\text{form}}, \tag{1}$$

where N_{elem} is the total number of elements in the system, c_i is the molar fraction of each element i, E_i is the molar energy of each element i, and ΔE_{form} is the formation energy. We predict the formation energy for each sample by subtracting the internal energy from the EAM-computed total energy. The formation energy is more directly related to the atomic configuration, and emphasizes the importance of an effective GCNN model for accurate predictions. The atomic arrangement makes the task of describing the material properties combinatorially complex; this represents the main difference from open source databases that have very broad elemental and mechanical coverage, but only include ordered compounds [47, 31, 32].

We calculated the elastic constants from all relaxed structures through LAMMPS. The elastic constants were evaluated based on an orthotropic symmetry by calculating the components of the stiffness tensor C_{11}, C_{22}, C_{33}, C_{12}, C_{13}, C_{23}, C_{44}, C_{55}, and C_{66}. The deformation strain was set to $\pm$ 0.1%. The components for the cubic crystal (C_{11}, C_{12}, C_{44}) were obtained by averaging the corresponding values. To estimate the upper and lower boundary of the properties for polycrystalline structures, the bulk modulus was calculated according to the Voigt (B_v) and Reuss (B_R) bounds for cubic crystals [48] by the following equations [49]:

$$B_V = \frac{C_{11} - C_{12} + 3C_{44}}{5} \tag{2}$$

$$B_R = \frac{5}{4S_{11} - 4S_{12} + 3S_{44}}, \tag{3}$$

where S_{ij} are the components of compliance tensor obtained from the inverse matrix of stiffness tensor. Then, the macroscale effective bulk modulus is estimated from the Voigt-Reuss-Hill approach as $B_{VRH} = (B_V + B_R^{-1})/2$ [48].

The original dataset contained a few crystal configurations with extreme values of the bulk modulus, which would have acted as outliers during the training of the GCNN model and negatively affected its predictive performance. To stabilize the GCNN training, we therefore pre-screened the dataset and removed any atomic configuration with a bulk modulus lower than 125.0 gigapascal (GPa) and higher than 1,000 GPa.

The range of values of the formation energy for the given configurations in the pre-screened dataset, expressed in units of electron Volt (eV), is $(-389.96, -159.78)$ and the range of values of the bulk modulus in units of gigapascal (GPa) is $(126.08, 237.53)$. Since different physical quantities have different units and different orders of magnitude, the inputs and outputs for each quantity are normalized between 0 and 1 across all data.

In Figure 2 we show the distribution of the formation energy and bulk modulus for atomic configurations by partitioning the data according to its initial regular BCC, FCC, and HCP crystal structures before applying geometry optimization. From the first row, we notice that the possible range of the formation energy is well represented by a large number of atomic configurations for each portion of the dataset based on the initial regular solid phase, although the distribution of atomic arrangements seems skewed towards energy values that are smaller in magnitude. Moreover, the scatter plots on the second row show that the

formation energy is strongly correlated with the chemical composition of the alloy. From the third row, we notice that the distribution of values of the bulk modulus has noticeable high peaked modes, indicating the values of the bulk modulus that occur most frequently across the possible set of atomic configurations. From the last row, we conclude that the dataset does not suggest any clear correlation between the value of the bulk modulus and the chemical composition of the alloy. These widespread scatter plots already suggest that predicting the bulk modulus as a function of the atomic arrangement may be a more challenging task than predicting the formation energy.

4. GCNN performance

We present numerical results that predict the formation energy and bulk modulus for or model systems of the binary Ni-Nb solid solution alloy system for the combined dataset containing BCC, FCC, and HCP crystal structures, as function of cutoff radius and using CGConv and PNAConv convolutional layer architectures.

4.1. Training setup

The architecture of the GCNN model has 10 graph convolutional layers with 100 neurons per layer. At first, we selected a radius cutoff of 5 Å to build the local neighborhoods used by the graph convolutional mask. We attach two FC layers at the end of the stack of convolutional layers, with 50 neurons in the first FC layer and 25 neurons in the second FC layer. Using the same GCNN architecture, two separate training procedures are performed, one to learn the formation energy and one to learn the bulk modulus. The GCNN models are trained using the Adam method [50] with a learning rate equal to 0.001, batch sizes of 32, and a maximum number of epochs set to 200. Early stopping is performed to interrupt the training when the validation loss function does not decrease for several consecutive epochs, as this is a symptom indicating that further epochs are very unlikely to reduce the value of the loss function. The training set for each of the NN represents 70% of the total dataset; the remaining portion of the data is equally split between validation and testing. As discussed in Section 3, compositional stratified splitting was performed to ensure that all the compositions were equally represented across training, validation, and testing datasets. The training of each DL model was performed on an NVIDIA V100 GPU.

4.2. Model accuracy and reliability

We conducted a series of "ablation studies" (one parameter is changed at a time) to monitor the change in predictive performance of our HydraGNN model with respect to the most important hyperparameters: policy of message passing performed by the graph convolutional layers, bond length as edge feature, and radius cut-off to define the local environment for information gathering. The mean absolute error (MAE) obtained by the HydraGNN models on the test dataset for predictions of both formation energy and bulk modulus are reported in Table 1. For both formation energy and bulk modulus, the computational time for training was on average 25,700 wall-clock seconds.

4.2.1. Influence of the message passing policy

The message passing policy used to transfer information across nodes in the graph significantly impacts the predictive accuracy of the HydraGNN model. The MAEs provided in Table 1 and the scatterplots included in the Supplementary Material show that PNAConv outperforms CGConv for both formation energy and bulk modulus, because the PNA better preserves graph isomorphism and thus better distinguishes different atomic disordered configurations.

4.2.2. Influence of the bond length as edge feature

The use of the bond length as edge features allows the graph convolutional layers to weigh the information passed across neighboring nodes based on their Euclidean distance. This additional information helps better discriminate between different crystal structures, thus enhancing the predictive power of model for accurate predictions of both formation energy and bulk modulus. This fact is confirmed both by the values of the test MAE reported in Table 1, as well as the scatterplots provided in the Supplementary Material.

Table 1: MAE for predictions of the formation energy and bulk modulus using CGConv and PNAConv for message passing in HydraGNN model.

Radius cut-off = 5.0 Å	**MAE - without edge features**	
Convolutional layer	**Formation energy**	**Bulk modulus**
CGConv	6.442 eV (0.141 eV/atom)	5.728 GPa
PNAConv	0.615 eV (0.013 eV/atom)	4.383 GPa
Radius cut-off = 5.0 Å	**MAE - bond length as edge feature**	
Convolutional layer	**Formation energy**	**Bulk modulus**
CGConv	6.074 eV (0.132 eV/atom)	5.724 GPa
PNAConv	0.474 eV (0.010 eV/atom)	3.242 GPa
Radius cut-off = 3.0 Å	**MAE - bond length as edge feature**	
Convolutional layer	**Formation energy**	**Bulk modulus**
CGConv	9.283 eV (0.210 eV/atom)	5.823 GPa
PNAConv	1.933 eV (0.041 eV/atom)	3.642 GPa
Radius cut-off = 6.9 Å	**MAE - bond length as edge feature**	
Convolutional layer	**Formation energy**	**Bulk modulus**
CGConv	3.519 eV (0.077 eV/atom)	5.644 GPa
PNAConv	0.529 eV (0.011 eV/atom)	3.436 GPa
Radius cut-off = 8.0 Å	**MAE - bond length as edge feature**	
Convolutional layer	**Formation energy**	**Bulk modulus**
CGConv	3.283 eV (0.072 eV/atom)	5.635 GPa
PNAConv	0.293 eV (0.006 eV/atom)	3.231 GPa

4.2.3. Influence of the radius cut-off for the local atomic environment

The local environment of an atom describes the region of the crystal inside which the interactions of an atom with neighboring atoms are non-negligible. In our HydraGNN model, the size of the local environment can be adjusted through the radius cut-off, which is a tunable hyperparameter. On the one hand, increasing the radius cut-off allows to retain more information about the local structure of the crystal, with potential benefits in the predictive performance of the model. On the other hand, larger values of the radius cut-off increase the number of parameters in the HydraGNN model, thus increasing the computational cost for training. In Table 1 we report the performance of the HydraGNN models using CGConv and PNAConv with values of the radius cut-off set to 3.0 Å, 5.0 Å, 6.9 Å, and 8.0 Å. The value 6.9 Å is considered because it corresponds to the value of the radius cut-off used by the EAM model that generated the training data. Although slight changes in the radius cut-off do not necessarily result in immediate changes of the predictive performance of the HydraGNN models, we can clearly see a change in performance comparing the results when the radius cut-off is equal to 3.0 Å and 8.0 Å, respectively. A very short cutoff radius of only 3.0 Å performs very poorly and has even problem predicting formation energies correctly with an MAE of 1.933 eV for the PNAConv architecture, whereas the improvement in extending the cutoff radius from 5.0 Å (MAE of 0.474 eV for PNAConv) to 8.0 Å (0.293 eV for PNAConv) with our computationally most expensive GCNN is less dramatic. The MAEs of the bulk modulus, on the other hand, are not varying smoothly as a function of the cutoff radius. This finding will be further discussed below.

Figure 3 shows the scatterplots that compare the predictions of formation energy and bulk modulus using the PNA convolutional layer with the bond length as edge feature and the radius cut-off set to 8.0 Å. A full comprehensive set of scatterplots for CGConv and PNAConv for all the values of the radius cut-off are provided in the Supplementary Material.

4.2.4. Restriction of bulk modulus predictions to the extremes of the compositional range

When we restrict the dataset to contain only data-samples for Nb concentrations below 0.2 and above 0.8, the predictive performance of the HydraGNN model to estimate the bulk modulus improves, attaining a test MAE equal to 1.9219 GPa. The scatterplot of the predictions is shown in Figure 4. This is indicative of the fact that structural displacements are less commonly occurring in more regularly ordered crystal structures, and therefore outliers are less common in these structures that conform to a more regular Ni or Nb crystal

lattice.

5. Discussion

For alloy design involving atomistic models, the search for metastable and disordered crystal structures during structural sampling is unavoidable. The enormous complexity of alloy structural variability requires the use of computationally inexpensive surrogate models trained on physics-based simulation methods. In this study, we tested the performance of graph-based neural network surrogate models in predicting the energies and bulk moduli for model systems of solid solution alloy systems. Our study shows the capabilities and limitations of state-of-the-art GCNN surrogate models, by training them on data generated with EAM potentials to inform future, more computationally expensive DFT-based surrogate model development. As expected from previous reports [51], the surrogate-predicted energy shows good agreement with ground truth data for all composition ranges. However, the predictions from the surrogate model for the bulk modulus of the solid solution alloy model systems were less satisfactory and failed to provide a measure of ranking between them when averaged over the entire composition range. The performance is considerably improved when limiting the composition space to binary mixtures systems having one dominant component (Ni concentration lower than 0.2 and higher than 0.8) with an associated MAE of 1.9219 GPa. We attribute the difficulty of prediction bulk modulus for binary alloys with comparable Ni:Nb ratio (Ni concentration between 0.2 and 0.8) to high variations of the bulk modulus in this region, possibly due to the fact that the EAM-optimized crystal structures are often metastable and correspond only to local minima.

The traditional methodology to computationally predict elasticity [52] is to apply different strain tensors on optimized atomic structures. However, an applied tensor can allow the system to escape from one local, metastable minimum to another, nearby minimum, which introduces deviations from a systematic exploration of structures in the elasticity calculations. These structural changes that occur during the calculation of a property for a given materials structure are unfortunately difficult to be captured correctly, using only energy-minimized structures. Unless a global geometry optimization scheme is employed for each alloy composition, the accuracy of elasticity predictions for a given structure is hard to improve even if more data was included, because it is difficult to tell just from atomic coordinates alone whether a certain structure is metastable or not.

We note that there might be a way to resolve this issue, namely by improving feature engineering. For example, a recent work tried to include the attention mechanism in the GCNN for crystal properties predictions [53]. Nevertheless, in that study, the resulting elasticity prediction improvement was not significant. Another approach might be to utilize the surrogate model to accurately predict atomic-scale potential energy surfaces, and to calculate elasticity by applying the strain tensors. Such an approach, similar in spirit to the neural network potentials by Behler and Parrinello [54], requires accurate predictions of stress from energy and volume under the deformation by the strain tensors. The generation of reference data in this way will likely require more effort and at least partial human supervision, in order to cover all of the configurational space.

6. Conclusion and future work

We have presented a GCNN model to predict the formation energy and the bulk modulus for the Ni-Nb solid solution binary alloy as a function of the atomic crystal lattice structure. The numerical results describe the predictive performance of the GCNN model on an open-source dataset for model systems of a binary Ni-Nb solid solution alloy [45], which spans a large variety of irregular crystal structures, each obtained as the result of a topology optimization starting from regular BCC, FCC, and HCP supercells. For each of the optimized crystal geometries, the formation energy and the bulk modulus as a prototypical elastic property are provided. Our PyTorch-based architecture that implements GCNN models, called HydraGNN, allows to flexibly switch between different graph convolutional layers implemented in PyTorch-Geometric that perform different message passing policies to aggregate information across adjacent nodes in the graph, and perform a cross-comparison. The PNAConv graph convolutional layer clearly outperforms the CGConv graph convolutional layer in all cases in terms of accuracy. The HydraGNN model using the PNAConv convolutional layer shows robustness in accurately predicting the formation energy over the diverse set of optimized lattice structures, which shows the potential of GCNN models of playing a pivotal role as effective

surrogate models in alloy design, since accurately estimating the formation energy is needed to identify the ensemble of stable crystal structures at a given chemical composition. We found that a radius cut-off larger than 5 Å significantly improves the predictive performance of the surrogate model for the prediction of the formation energy. The HydraGNN performance for predicting the bulk modulus seems less dependent on the cutoff radius, as large structural variations and number of local minima in intermediate concentration ranges between 0.2 and 0.8 of element composition dramatically increase. Therefore, the fidelity of bulk modulus evaluations is lower than for the formation energy, which in turn limits the attainable accuracy of the GCNN model to predicting the former compared to the latter. Similar to the bulk modulus, one can obtain phonon dispersion or phonon density of states (DOS). As we observed the trend in our bulk modulus calculations, the phonon dispersion and PDOS were relatively well predicted at low or high mixing ratios because in these regions the calculation basically is dominated by the deformation matrix.

For future work, a partial improvement of the predictions may be obtained by generating a new dataset where the topology optimization is run with more stringent convergence requirements to ensure that the final crystal structure is fully relaxed. In fact, for some of the crystal structures contained in the current dataset, convergence was not fully reached since the bulk modulus is more sensitive to small changes in geometry than the formation energy. Therefore, the fidelity of bulk modulus evaluations is lower than for the formation energy, which in turn limits the attainable accuracy of the HydraGNN model to predicting the former compared to the latter. Additional improvement in the predictions of the bulk modulus may also be obtained by including additional input features, both geometric features describing the overall crystal structure (e.g., angles) as well as chemical features for each atom species (e.g., valence electrons, electronegativity/electropositivity, atomic mass, atom size), fed into the HydraGNN model.

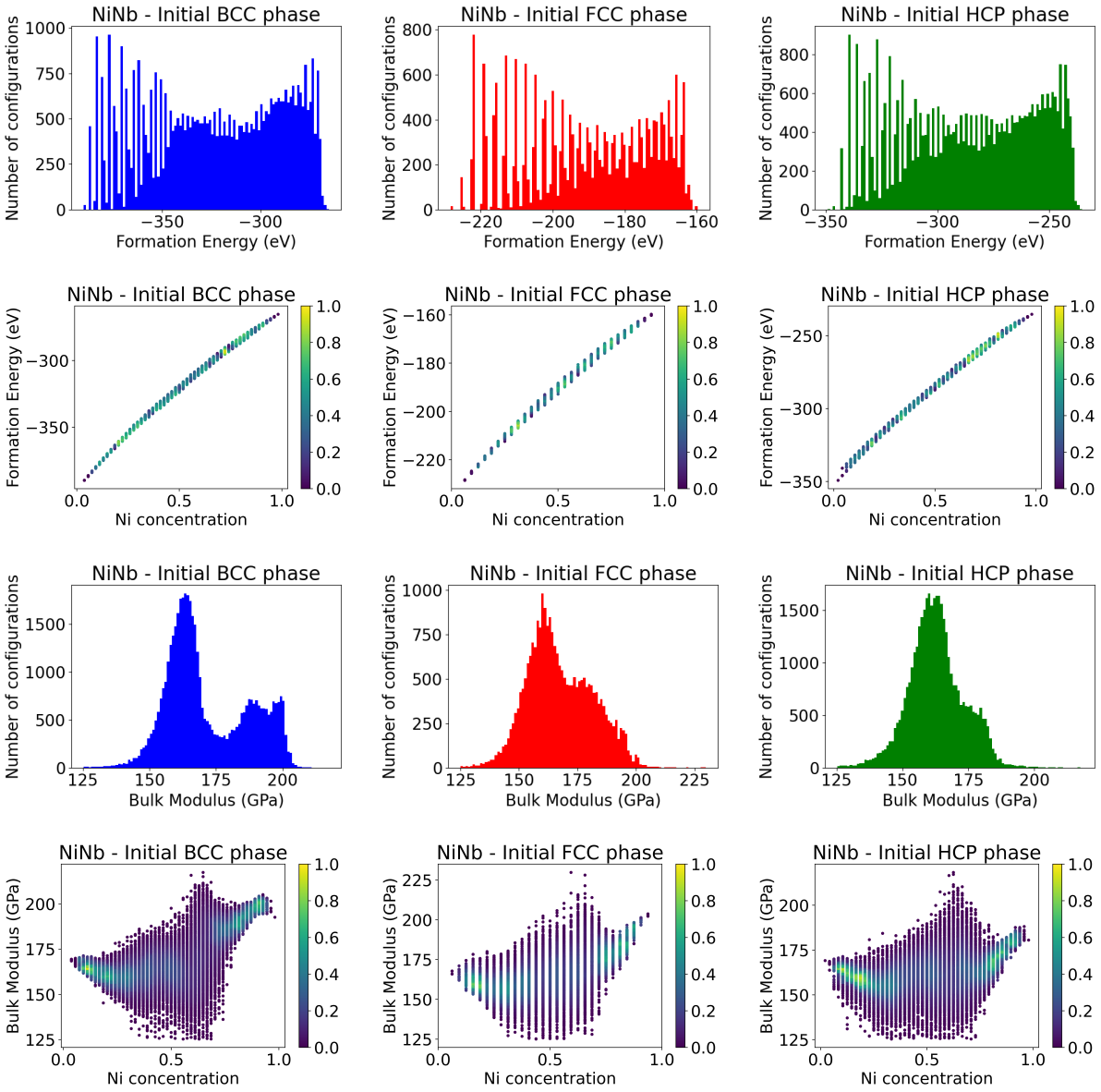

Figure 2: Illustration for the Ni-Nb dataset with multiple crystal structures. The figures describe the distribution of values of the formation energy and bulk modulus on optimized irregular geometries. The illustrations are split based on the type of regular crystal structure used as initial guess to perform geometry optimization: initial BCC phase (left column), initial FCC phase (centered column), and initial HCP phase (right column). First row: histograms of values of the formation energy. Second row: scatter plot of the formation energy as a function of Ni concentration. Third row: histograms of values of the bulk modulus. Fourth row: scatter plot of the bulk modulus. The colormap describes the density of points.

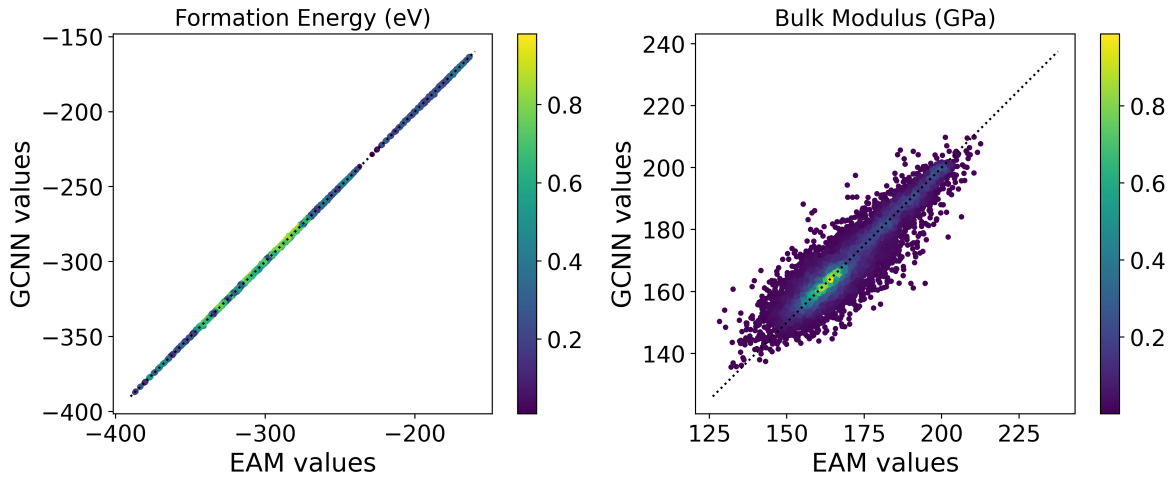

Figure 3: Scatter plot of the GCNN-PNAConv predictions (using bond length as input edge feature and radius cut-off set to 8.0 Å) of the formation energy (left) and of the bulk modulus (right) against the respective target EAM values using the entire dataset. The colormap describes the density of points.

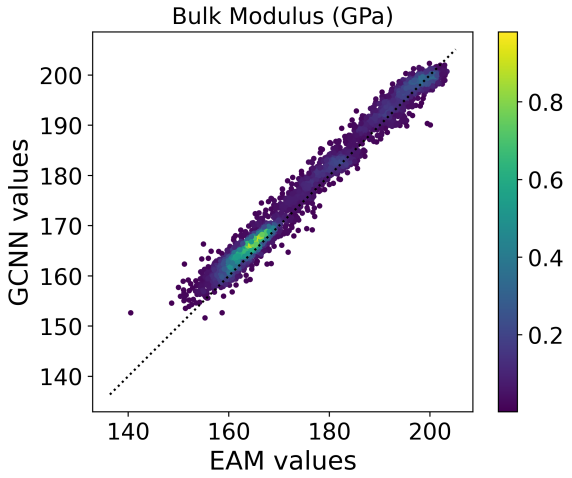

Figure 4: Scatter plot of the GCNN-PNAConv predictions (using bond length as edge feature and radius cut-off set to 5.0 Å) of the bulk modulus against the respective target EAM values only for data related to chemical composition of Nb below 0.2 and above 0.8. The colormap describes the density of points.

Acknowledgements

The authors thank Dr. Vladimir Protopopescu for his valuable feedback in the preparation of this manuscript. This work was supported in part by the Office of Science of the Department of Energy and by the Laboratory Directed Research and Development (LDRD) Program of Oak Ridge National Laboratory. This research is sponsored by the Artificial Intelligence Initiative as part of the Laboratory Directed Research and Development (LDRD) Program of Oak Ridge National Laboratory, managed by UT-Battelle, LLC, for the US Department of Energy under contract DE-AC05-00OR22725. An award of computer time was provided by the OLCF Director's Discretion Project program using the OLCF award MAT250. This work used resources of the Oak Ridge Leadership Computing Facility and of the Edge Computing program at the Oak Ridge National Laboratory, which is supported by the Office of Science of the U.S. Department of Energy under Contract No. DE-AC05-00OR22725.

Data availability

The solid solution binary alloy NiNb dataset [45] related to this article can be found at `https://www.osti.gov/dataexplorer/biblio/dataset/1890159`, an open-source online data repository hosted at U.S. Department of Energy Office of Scientific and Technical Information.

Code availability

The open-source HydraGNN library [42] used to generate the numerical results described in this article can be accessed at the following GitHub repository `https://github.com/ORNL/HydraGNN`.

References

[1] D. Xue, P. V. Balachandran, J. Hogden, J. Theiler, D. Xue, and T. Lookman. Accelerated search for materials with targeted properties by adaptive design. *Nature Communications*, 7(11241), April 2016.

[2] Y. Wang, B. Goh, P. Nelaturu, T. Duong, N. Hassan, R. David, M. Moorehead, S. Chaudhuri, A. Creuziger, J. Hattrick-Simpers, D. J. Thoma, K. Sridharan, and A. Couet. Integrated high-throughput and machine learning methods to accelerate discovery of molten salt corrosion-resistant alloys. *Advanced Science*, page 2200370, 2022.

[3] G. L. W Hart, T. Mueller, C. Toher, and S. Curtarolo. Machine learning for alloys. *Nature Reviews Materials*, 6(8):730–755, 2021.

[4] B. D Conduit, N. G Jones, H. J Stone, and G. J. Conduit. Design of a nickel-base superalloy using a neural network. *Materials & Design*, 131:358–365, 2017.

[5] L. Kaufman and H. Bernstein. Computer calculation of phase diagrams. with special reference to refractory metals. 1970.

[6] N. Saunders and A. P. Miodownik. *CALPHAD (calculation of phase diagrams): a comprehensive guide*. Elsevier, 1998.

[7] F. Monji and M. A. Jabbareh. Thermodynamic model for prediction of binary alloy nanoparticle phase diagram including size dependent surface tension effect. *Calphad*, 58:1–5, 2017.

[8] P. Laiu, Y. Yang, M. Lupo Pasini, J. Y. Choi, and D. Shin. A neural network approach to predict gibbs free energy of ternary solid solutions. *arXiv preprint arXiv:2209.05609*, 2022.

[9] S. Bigdeli, L.-F. Zhu, A. Glensk, B. Grabowski, B. Lindahl, T. Hickel, and M. Selleby. An insight into using dft data for calphad modeling of solid phases in the third generation of calphad databases, a case study for al. *Calphad*, 65:79–85, 2019.

[10] Q. Liu, X.-G. Lu, P. Boulet, M. C. Record, and Q.-M. Hu. Influence of atomic order on the enthalpy of formation and bulk modulus of the sigma phase. *Fluid Phase Equilibria*, 459:238–243, 2018.

[11] P. Pluengphon, P. Wanarattikan, T. Bovornratanaraks, and B. Inceesungvorn. Pressure-induced formation of quaternary compound and in-N distribution in InGaAsN zincblende from ab initio calculation. *Chemistry Open*, 8(3):393–398, 2019.

[12] Q. Liu, X.-G. Lu, P. Boulet, M. C. Record, and Q.-M. Hu. On the importance of hexagonal phases in TM (TM=Ti, Zr, and Hf) mono-nitrides. *Journal of Applied Physics*, 128(105106), 2020.

[13] G. Yao, W. Y. Wang, C. Zou, K. Ren, P. Li, X. Gao, D. Lin, J. Wang, S. Yang, Y. Wang, H. Song, and J. Li. Local orders, lattice distortions, and electronic structure dominated mechanical properties of (ZrHfTaM1M2)C (M = Nb, Ti, V). *Journal of the American Ceramic Society*, 105(6):4260–4276, 2020.

[14] A. Jain, S. P. Ong, G. Hautier, W. Chen, W. D. Richards, S. Dacek, S. Cholia, D. Gunter, D. Skinner, G. Ceder, and K. A. Persson. Commentary: The materials project: A materials genome approach to accelerating materials innovation. *APL materials*, 1(1):011002, 2013.

[15] S. Kirklin, J. E Saal, B. Meredig, A. Thompson, J. W. Doak, M. Aykol, S. Rühl, and C. Wolverton. The open quantum materials database (oqmd): assessing the accuracy of dft formation energies. *npj Computational Materials*, 1(1):1–15, 2015.

[16] S. Curtarolo, W. Setyawan, S. Wang, J. Xue, K. Yang, R. H Taylor, L. J Nelson, G. L. W Hart, S. Sanvito, M. Buongiorno-Nardelli, N. Mingo, and O. Levy. Aflowlib. org: A distributed materials properties repository from high-throughput ab initio calculations. *Computational Materials Science*, 58:227–235, 2012.

[17] J. M. Sanchez, F. Ducastelle, and D. Gratias. Generalized cluster description of multicomponent systems. *Phys. A Stat. Mech. Appl.*, 128:334–350, 1984.

[18] S. Gorsse and F. Tancret. Current and emerging practices of calphad toward the development of high entropy alloys and complex concentrated alloys. *Journal of Materials Research*, 33(19):2899–2923, 2018.

[19] A. Van de Walle, G. Ceder, and U. V. Waghmare. First-principles computation of the vibrational entropy of ordered and disordered ni 3 al. *Physical Review Letters*, 80(22):4911, 1998.

[20] M. Widom, W. P. Huhn, S. Maiti, and W. Steurer. Hybrid monte carlo/molecular dynamics simulation of a refractory metal high entropy alloy. *Metallurgical and Materials Transactions A*, 45(1):196–200, 2014.

[21] W.-M. Choi, Y. H. Jo, S. S. Sohn, S. Lee, and B.-J. Lee. Understanding the physical metallurgy of the cocrfemnni high-entropy alloy: an atomistic simulation study. *npj Computational Materials*, 4(1):1–9, 2018.

[22] J. Maguire, M. Benedict, L. Woodcock, and S. LeClair. Artificial intelligence in materials science: Application to molecular and particulate simulations. *MRS Commun.*, 700(S8.1.):10.1557/mrc.2019.95, 2001.

[23] R. K. Vasudevan, K. Choudhary, A. Mehta, R. Smith, G. Kusne, F. Tavazza, L. Vlcek, M. Ziatdinov, S. V. Kalinin, and J. Hattrick-Simpers. Materials science in the AI age: high-throughput library generation, machine learning and a pathway from correlations to the underpinning physics. *MRS Commun.*, 9(3):10.1557/mrc.2019.95, 2019.

[24] W. Sha, Y. Guo, Q. Yuan, S. Tang, X. Zhang, S. Lu, X. Guo, Y.-C. Cao, and S. Cheng. Artificial intelligence to power the future of materials science and engineering. *Advanced Intelligent Systems*, 2(4):1900143, 2020.

[25] D. Morgan and R. Jacobs. Opportunities and challenges for machine learning in materials science. *Annual Review of Materials Research*, 50:71–103, 2020.

[26] M. W. Gaultois, A. O. Oliynyk, A. Mar, T. D. Sparks, G. J. Mulholland, and B. Meredig. Perspective: Web-based machine learning models for real-time screening of thermoelectric materials properties. *APL Materials*, 4(053213), May 2016.

[27] S. Lu, Q. Zhou, Y. Ouyang, Y. Guo, and J. Li, Q.; Wang. Accelerated discovery of stable lead- free hybrid organic-inorganic perovskites via machine learning. *Nature Communications*, 9(3405), August 2018.

[28] R. Gómez-Bombarelli. Design of efficient molecular organic light-emitting diodes by a high-throughput virtual screening and experimental approach. *Nature Materials*, 15:1120–1127, August 2016.

[29] T. Xie and J. C. Grossman. Crystal graph convolutional neural networks for an accurate and interpretable prediction of material properties. *Phys. Rev. Lett.*, 120(14):145301, April 2018.

[30] C. Chen, W. Ye, Y. Zuo, C. Zheng, and S. P. Ong. Graph networks as a universal machine learning framework for molecules and crystals. *Chem. Mater.*, 31(9):3564–3572, May 2019.

[31] A. Jain, S. Ping Ong, G. Hautier, W. Chen, W. D. Richards, S. Dacek, S. Cholia, D. Gunter, D. Skinner, G. Ceder, and K. A. Persson. Commentary: The materials project: A materials genome approach to accelerating materials innovation. *APL Mater.*, 1(1):0–11, 2013.

[32] J. E Saal, S. Kirklin, M. Aykol, B. Meredig, and C. Wolverton. Materials design and discovery with high-throughput density functional theory: the Open Quantum Materials Database (OQMD). *JOM*, 65(11):1501–1509, November 2013.

[33] M. Lupo Pasini and M. Eisenbach. CuAu binary alloy with 32 atoms - LSMS-3 data - DOI:10.13139/OLCF/1765349. 2 2021.

[34] M. Lupo Pasini and M. Eisenbach. FePt binary alloy with 32 atoms - LSMS-3 data - DOI:10.13139/OLCF/1762742. 2 2021.

[35] M. Lupo Pasini, M. Burĉul, S. T. Reeve, M. Eisenbach, and S. Perotto. Fast and accurate predictions of total energy for solid solution alloys with graph convolutional neural networks. *Springer Journal of Communications in Computer and Information Science*, 1512, September 2021.

[36] M. Lupo Pasini, P. Zhang, S. T Reeve, and J. Y. Choi. Multi-task graph neural networks for simultaneous prediction of global and atomic properties in ferromagnetic systems. *Mach. learn.: sci. technol.*, 3(2):025007, may 2022.

[37] M. S. Daw, S. M. Foiles, and M. I. Baskes. The embedded-atom method: a review of theory and applications. *Materials Science Reports*, 9(7-8):251–310, 1993.

[38] F. Scarselli, M. Gori, A. C. Tsoi, M. Hagenbuchner, and G. Monfardini. The graph neural network model. *IEEE Transactions on Neural Networks*, 20(1):61–80, 2009.

[39] M. Defferrard, X. Bresson, and P. Vandergheynst. Convolutional neural networks on graphs with fast localized spectral filtering. In D. Lee, M. Sugiyama, U. Luxburg, I. Guyon, and R. Garnett, editors, *Advances in Neural Information Processing Systems*, volume 29. Curran Associates, Inc., 2016.

[40] G. Corso, L. Cavalleri, D. Beaini, P. Liò, and P. Veličković. Principal neighbourhood aggregation for graph nets. *arXiv:2004.05718 [cs, stat]*, December 2020. arXiv: 2004.05718.

[41] PyTorch Geometric. `https://pytorch-geometric.readthedocs.io/en/latest/`.

[42] M. Lupo Pasini, S. T. Reeve, P. Zhang, and J. Y. Choi. HydraGNN. [Computer Software] `https://doi.org/10.11578/dc.20211019.2`, oct 2021.

[43] B. J. Piearcey, R. Jackson, and B. B. Argent. The mechanical properties and structure of cobalt-nickel-niobium alloys. *J. Inst. Metals*, 91, 1963.

[44] Y. Zhang, R. Ashcraft, M. I. Mendelev, C. Z. Wang, and K. F. Kelton. Experimental and molecular dynamics simulation study of structure of liquid and amorphous $Ni_{62}Nb_{38}$ alloy. *The Journal of Chemical Physics*, 145(20):204505, 2016.

[45] GS Jung, M. Lupo Pasini, and S. Irle. ORNL_AISD_NiNb - DOI:10.13139/OLCF/1890159. 10 2022.

[46] A. P. Thompson, H. M. Aktulga, R. Berger, D. S. Bolintineanu, W. M. Brown, P. S. Crozier, P. J. in 't Veld, A. Kohlmeyer, S. G. Moore, T. D. Nguyen, R. Shan, M. J. Stevens, J. Tranchida, C. Trott, and S. J. Plimpton. LAMMPS - a flexible simulation tool for particle-based materials modeling at the atomic, meso, and continuum scales. *Comp. Phys. Comm.*, 271:108171, 2022.

[47] S. Curtarolo, W. Setyawan, G. L. W. Hart, M. Jahnatek, R. V. Chepulskii, R. H. Taylor, S. Wang, J. Xue, K. Yang, O. Levy, M. J. Mehl, H. T. Stokes, D. O. Demchenko, and D. Morgan. AFLOW: An automatic framework for high-throughput materials discovery. *Comput. Mater. Sci.*, 58:218–226, June 2012.

[48] L. Zuo, M. Humbert, and C. Esling. Elastic properties of polycrystals in the voigt-reuss-hill approximation. *Journal of Applied Crystallography*, 25(6):751–755, 1992.

[49] J. M. J Den Toonder, J. A. W. Van Dommelen, and F. P. T Baaijens. The relation between single crystal elasticity and the effective elastic behaviour of polycrystalline materials: theory, measurement and computation. *Modelling and Simulation in Materials Science and Engineering*, 7(6):909, 1999.

[50] Diederik P. Kingma and Jimmy Ba. Adam: a method for stochastic optimization. *arXiv:1412.6980 [cs]*, January 2017. arXiv: 1412.6980.

[51] M. De Jong, W. Chen, R. Notestine, K. Persson, G. Ceder, A. Jain, M. Asta, and A. Gamst. A statistical learning framework for materials science: application to elastic moduli of k-nary inorganic polycrystalline compounds. *Scientific Reports*, 6(1):1–11, 2016.

[52] M. De Jong, W. Chen, T. Angsten, A. Jain, R. Notestine, A. Gamst, M. Sluiter, C. Krishna Ande, S. Van Der Zwaag, J. J Plata, T. Coher, S. Curtarolo, G. Ceder, K. A. Persson, and M. Asta. Charting the complete elastic properties of inorganic crystalline compounds. *Scientific data*, 2(1):1–13, 2015.

[53] S.-Y. Louis, Y. Zhao, A. Nasiri, X. Wang, Y. Song, F. Liu, and J. Hu. Graph convolutional neural networks with global attention for improved materials property prediction. *Physical Chemistry Chemical Physics*, 22(32):18141–18148, 2020.

[54] J. Behler and M. Parrinello. Generalized neural-network representation of high-dimensional potential-energy surfaces. *Physical Review Letters*, 98(14):146401, 2007.